



A Mathematical Model of the Lead-Acid Battery to Address the Effect of Corrosion

Vijayasekaran Boovaragavan,^{***} Ravi N. Methakar,
Venkatsailanathan Ramadesigan,^{*} and Venkat R. Subramanian^{***,z}

Department of Energy, Environment and Chemical Engineering Washington University in Saint Louis, Saint Louis, Missouri 63130, USA

A mathematical model of the lead-acid battery is developed with due consideration for the corrosion process that occurs at the interface between the active material and grid material of the positive plate. Three different modeling approaches are used to incorporate the effect of corrosion in the first-principles-based porous electrode model of the lead-acid cell. These approaches are used to examine the effects of corrosion during discharge, rest, and charge processes. First, the electronic conductivity of the positive plate is empirically expressed as a function of N , the number of cycles, next an current-resistance loss term to account for the increase in electronic resistance due to the formation and growth of passive corrosion layer is considered, and finally the corrosion phenomenon is incorporated as a side reaction occurring in the positive plate. It is identified that the modeling approach used in this work can be used to investigate the effect of corrosion on lead-acid battery performances.
© 2009 The Electrochemical Society. [DOI: 10.1149/1.3190510] All rights reserved.

Manuscript submitted March 20, 2009; revised manuscript received July 7, 2009. Published September 3, 2009.

Secondary batteries are widely used in portable consumer devices, uninterruptible power supplies, as automobile starters, and in emerging applications like transportation, space, and military. However, there are still some poorly understood processes, like the corrosion of positive plate in lead-acid batteries and capacity fade in lithium-ion batteries that force limitations to promote secondary batteries in these emerging applications. Lead-acid battery technology has been successfully serving for different energy needs that vary from the requirements for traditional automobile industry to modern plug-in hybrid electric vehicles. Though other battery technologies (lithium ion, nickel, cadmium, etc.) might have an edge over this technology for some specific applications like in electronic devices and high power applications, lead-acid battery technology has many advantages as starting, lighting, and ignition battery in automobile industries that cannot be replaced with any other existing technology. But, one of the major failure mechanisms in this technology is the formation and buildup of passive corrosion layer at the interface between the active material and grid material of the positive plate. This process significantly influences the battery operation because the electrons generated at the positive active materials need to overcome additional resistances to flow through positive grid material and reach the external circuit. Various positive plate materials that use alloy of different metals and metallic oxides are still being investigated to avoid the passive corrosion layer formation and growth. Modeling this intrinsic process can greatly help in understanding the failure mechanism.

Many detailed models for lead-acid batteries have been reported.¹⁻¹⁷ These models are typically one dimensional and include a detailed description of the physical, chemical, and electrical processes that take place in the battery. Efforts in recent years have focused on modeling the behavior of valve-regulated lead-acid batteries which have become increasingly important in commercial applications. One can see that some models are based on the search for analytical solutions of the diffusion equation combined with an electrical circuit.¹⁻⁶ More recent electrochemical engineering models rely heavily on the solution of similar equation sets by numerical simulation.⁷⁻¹⁷ This permits researchers to study a large range of parameters involved.

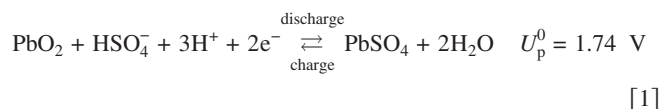
There are a few articles that address the failure of the lead-acid battery due to corrosion at the positive plate.¹⁸⁻²² Pavlov¹⁹ provided various possible mechanisms for the formation of corrosion layer with experimental evidences. Perhaps the first mathematical evalu-

ation of the corrosion layer formation at the positive plate was reported by Ball et al.^{20,21} However, it considered a general three-dimensional Laplace equation that does not address change in process variables such as electrolyte concentration, porosity, etc. Recently, Osório et al.²² analyzed the effects of the microstructural morphologies of an alloy on the resulting corrosion resistance in H₂SO₄ solution at different temperatures and other process conditions. Thus, the modeling corrosion mechanism in a lead-acid cell has not been addressed in detail in the literature. This paper attempts to develop a mathematical model that accounts for the effects of passive corrosion layer in the lead-acid battery. In light of this, three different approaches are made to address the corrosion mechanism. A comparison between discharge and charge profiles from the model with and without corrosion shows that this modeling approach can be used to study the effect of corrosion on lead-acid battery performances.

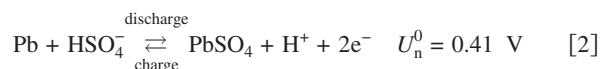
Formulation of the Mathematical Model

The modeling framework.—The mathematical model derived here is based on the four-layer geometry of a flooded lead-acid cell, as shown in Fig. 1. It consists of a porous lead dioxide electrode as a positive plate, an electrolyte reservoir, a separator, and another porous electrode as a negative plate made out of spongy lead. When this cell is discharged, an electron current flows from the negative electrode to the positive electrode through an external load connected across the negative and positive terminals. The fundamental electrode reactions at the matrix-electrolyte interface that cause the flow of this electron current is given as follows.²³

PbO₂ electrode



Pb electrode



A mathematical model for this system is reported in detail in this paper with an explanation for governing equations, boundary and initial conditions, and specification of expressions for transport and kinetics inside the cell. This is done to provide clarity for comparing different approaches to address the effect of corrosion. The model does not consider all the geometric details of the porous electrode but it does consider all the necessary features essential for the simulation of electrode performance. The assumptions involved in the model formulation are as follows. (i) The system is considered to be

* Electrochemical Society Student Member.

** ECS Oronzio de Nora Industrial Electrochemistry Fellowship Award Recipient.

*** Electrochemical Society Active Member.

^z E-mail: vsbramania@seas.wustl.edu

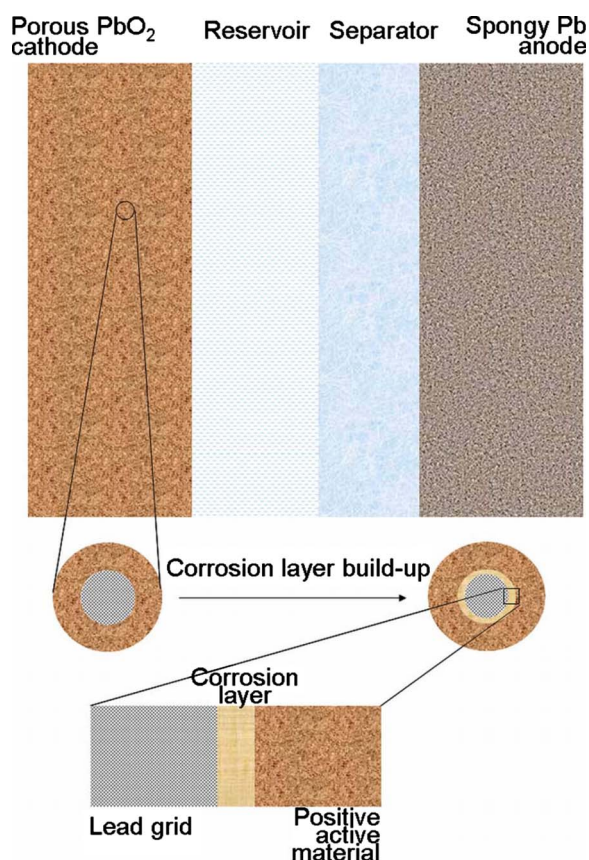


Figure 1. (Color online) Schematic of a flooded lead-acid cell with corrosion layer formation.

one dimensional. (ii) Porous electrodes are assumed to be macro-homogeneous where the pores between the solid and liquid phases are completely filled with the acid electrolyte. (iii) The sulfuric acid is a binary electrolyte, where it dissociates only into two ions, HSO_4^- and H^+ , in the solvent H_2O . (iv) The cell is considered to be isothermal during its operation.

Model equations.—Material balance for electrolyte concentration.—The differential material balance for a dissolved species i is expressed as²⁴

$$\frac{\partial(\epsilon c)}{\partial t} = -\frac{\partial N_{x,i}}{\partial x} + R_i \quad \text{where } i = +, -, \text{ and } 0(\text{solvent}) \quad [3]$$

where $N_{x,i}$ is the flux and R_i is the electrochemical reaction rate. The flux term can be expressed as the sum of convection, diffusion, and migration⁹⁻¹²

$$N_{x,i} = c_i \bar{V} - D_{\text{eff}} \frac{\partial c_i}{\partial x} + \frac{t_i^0}{z_i F} i_2 \quad \text{where } i = +, - \quad [4]$$

$$N_{x,0} = c_0 \bar{V} - D_{\text{eff}} \frac{\partial c_0}{\partial x} \quad [5]$$

Using the relationships between the concentration of the electrolyte and those of its dissociated ions and the solvent ($c = c_+/n_+ = c_-/n_-$), the material balance on the electrolyte concentration c can be written as

$$\epsilon \frac{\partial c}{\partial t} + \bar{V} \frac{\partial c}{\partial x} = \frac{\partial}{\partial x} \left(D \epsilon^{\text{exl}} \frac{\partial c}{\partial x} \right) + \left[-\frac{s_+}{v_+ n F} - \frac{t_+^0}{v_+ z_+ F} + \frac{c}{n F} \right. \\ \left. \times \left(\frac{s_+ \bar{V}_e}{v_+} + \frac{n t_+^0 \bar{V}_e}{v_+ z_+} + s_0 \bar{V}_0 \right) \right] j \quad [6]$$

where \bar{V} is the volume average velocity and its expression can be derived from the concept of conservation of volume.⁹⁻¹² This can be expressed as

$$\bar{V} = -\frac{1}{n F} \left(\frac{s_+ \bar{V}_e}{v_+} + \frac{n t_+^0 \bar{V}_e}{v_+ z_+} + s_0 \bar{V}_0 + \sum_k^{\text{solid species}} \frac{s_k M_k}{\rho_k} \right) i_2 \quad [7]$$

where n is the number of electrons involved in the electrode reaction which is equal to 2, s_i is the stoichiometric coefficient of species i in an electrode reaction written in Newman's standard notation, z_i is the charge number of ion i ($z_+ = z_- = 1$), and v_i is the dissociation coefficient of species i . For the binary electrolyte, H_2SO_4 , which dissociates into HSO_4^- and H^+ the dissociation coefficients are $v_+ = v_- = 1$. The values for the stoichiometric coefficients in the material balance equation of the electrolyte concentration depend on the electrochemical reaction (Eq. 1 and 2) that takes place in each region of the cell, as shown in Fig. 1. Values of the coefficients used in the governing equations for electrolyte concentration for the positive electrode and reservoir are $s_+ = -3$, $s_0 = 2$, $s_{\text{PbSO}_4} = 1$, and $s_{\text{PbO}_2} = -1$. Values of the coefficients used in the governing equations for electrolyte concentration for the negative electrode and separator are $s_+ = -1$, $s_0 = 0$, $s_{\text{PbSO}_4} = -1$, and $s_{\text{Pb}} = 1$. After the substitution of these values followed by rearranging the terms, the governing equations for electrolyte concentration in all four regions of a lead-acid cell are given in Table I.

Material balance for porosity variations.—Changes in electrode porosity can be expressed in terms of volume differences between solid reactants and products. This can be expressed as

$$\frac{\partial \epsilon}{\partial t} = \frac{1}{n F} \sum_k^{\text{solid species}} \frac{s_k M_k}{\rho_k} \frac{\partial i_2}{\partial x} \quad [8]$$

The governing equation for porosity variation at each electrode after substituting for stoichiometric coefficients is given in Table I.

Ohm's law for the electrolyte.—From the use of concentrated solutions theory and measuring the solution potential using a reference electrode of the same kind as the porous electrode, the current density of the binary electrolyte can be expressed as a sum of electrical and electrochemical potentials²⁴

$$\frac{i_2}{\kappa_{\text{eff}}} = -\frac{\partial \Phi_2}{\partial x} - \left(\frac{s_+}{v_+ n F} + \frac{t_+^0}{v_+ z_+ F} - \frac{s_0 c}{n F c_0} \right) \frac{\partial \mu_e}{\partial x} \quad [9]$$

The electrochemical potential of the electrolyte can be expressed as

$$\mu_e = \nu R T \ln(cf) \quad [10]$$

where f is the mean activity coefficient and c_0 is the solvent concentration. The resulting Ohm's law for the electrolyte is

$$\frac{i_2}{\kappa_{\text{eff}}} = -\frac{\partial \Phi_2}{\partial x} - \frac{\nu R T}{F} \left(\frac{s_+}{v_+ n} + \frac{t_+^0}{v_+ z_+} - \frac{s_0 c \bar{V}_0}{n(1 - c \bar{V}_e)} \right) \frac{\partial \ln(cf)}{\partial x} \quad [11]$$

The coefficients s_+ , s_- , s_0 , and n correspond to those associated with the reaction occurring at the respective electrode. The final governing equations for the electrolyte potential in each region of the lead-acid cell are given in Table I.

Ohm's law for solid phase.—For the solid phase, Ohm's law can be represented by the following expression²⁴

Table I. Governing equations for the lead-acid battery model.

Region	Governing equations
Positive plate	$\varepsilon \frac{\partial c}{\partial t} = \frac{\partial}{\partial x} \left(\varepsilon^{\text{ex1}} D \frac{\partial c}{\partial x} \right) + \left(\frac{(3 - 2t_+)(1 - cV_e)}{2F} + \frac{cV_0}{F} \right) j_p + \left(\frac{a_1 - (3 - 2t_+)V_e + 2V_0}{2F} i_2 \right) \frac{\partial c}{\partial x}$ $- \varepsilon^{\text{ex1}} \sigma_{\text{PbO}_2} \frac{\partial \Phi_1}{\partial x} - \varepsilon^{\text{ex1}} \kappa \frac{\partial \Phi_2}{\partial x} + \varepsilon^{\text{ex1}} \kappa \frac{RT}{F} (1 - 2t_+) \frac{\partial \ln fc}{\partial x} = I_{\text{app}}$ $\varepsilon^{\text{ex1}} \sigma_{\text{PbO}_2} \frac{\partial^2 \Phi_1}{\partial x^2} = j_p$ $\frac{\partial \varepsilon}{\partial t} = \frac{a_1 j_p}{2F}$ $i_2 = I_{\text{app}} + \varepsilon^{\text{ex1}} \sigma_{\text{PbO}_2} \frac{d\Phi_1}{dx}$
Reservoir	$\frac{\partial c}{\partial t} = D \frac{\partial^2 c}{\partial x^2} + \left(\frac{a_1 - (3 - 2t_+)V_e + 2V_0}{2F} I_{\text{app}} \right) \frac{\partial c}{\partial x}$ $- \kappa \frac{\partial \Phi_2}{\partial x} + \kappa \frac{RT}{F} (1 - 2t_+) \frac{\partial \ln fc}{\partial x} = I_{\text{app}}$
Separator	$\varepsilon_{\text{sep}} \frac{\partial c}{\partial t} = \varepsilon_{\text{sep}}^{\text{ex3}} D \frac{\partial^2 c}{\partial x^2} - \left(\frac{a_2 + (1 - 2t_+)V_e}{2F} I_{\text{app}} \right) \frac{\partial c}{\partial x}$ $- \varepsilon_{\text{sep}}^{\text{ex3}} \kappa \frac{\partial \Phi_2}{\partial x} + \varepsilon_{\text{sep}}^{\text{ex3}} \kappa \frac{RT}{F} (1 - 2t_+) \frac{\partial \ln fc}{\partial x} = I_{\text{app}}$
Negative plate	$\varepsilon \frac{\partial c}{\partial t} = \frac{\partial}{\partial x} \left(\varepsilon^{\text{ex4}} D \frac{\partial c}{\partial x} \right) + \frac{(1 - 2t_+)(1 - cV_e)}{2F} j_n + \left(\frac{a_2 - (1 - 2t_+)V_e}{2F} i_2 \right) \frac{\partial c}{\partial x}$ $- \varepsilon^{\text{ex4}} \sigma_{\text{Pb}} \frac{\partial \Phi_1}{\partial x} - \varepsilon^{\text{ex4}} \kappa \frac{\partial \Phi_2}{\partial x} + \varepsilon^{\text{ex4}} \kappa \frac{RT}{F} (1 - 2t_+) \frac{\partial \ln fc}{\partial x} = I_{\text{app}}$ $\varepsilon^{\text{ex4}} \sigma_{\text{Pb}} \frac{\partial^2 \Phi_1}{\partial x^2} = j_n$ $\frac{\partial \varepsilon}{\partial t} = \frac{a_2 j_n}{2F}$ $i_2 = I_{\text{app}} + \varepsilon^{\text{ex4}} \sigma_{\text{Pb}} \frac{d\Phi_1}{dx}$

$$i_1 = -\varepsilon^{\text{exm}} \sigma \frac{\partial \Phi_1}{\partial x} \quad [12]$$

where the factor exm is used to account for the tortuosity. The governing equation for solid phase electric potential in each porous electrode is given in Table I.

Conservation of charge.— Under the assumption of electroneutrality, the conservation of charge for a macroscopic model can be expressed as

$$\frac{\partial i_1}{\partial x} + \frac{\partial i_2}{\partial x} = 0 \quad [13]$$

where i_1 and i_2 are current densities in the solid phase and the liquid phase, respectively. Because the conservation of charge has to be maintained, at the center of the electrode, all the current in the cell is in the current collector and at the interfaces $x = l_p$ (electrode/reservoir), all the current in the cell is in the electrolyte because

there is no active solid phase beyond this interface. Using these conditions, Eq. 13 can be written as

$$i_1 + i_2 = i_{\text{app}} \quad [14]$$

Electrokinetics.— The rate of the electrochemical reaction at the porous electrode depends on the (i) interfacial surface area available for the electrode reaction a , which continuously changes due to the production of PbSO_4 during discharge and Pb or PbO_2 during charge, (ii) local electrolyte concentration c governed by Eq. 6; (iii) exchange current density i_0 measured at a specific concentration and temperature; (iv) temperature T , which is assumed to be a constant at 25°C ; and (v) electrode overpotential η , this is the difference between the electrical potential in the solid phase and that in the liquid phase and open-circuit potential expressed as $\eta = \Phi_1 - \Phi_2 - U$. This can be expressed in the form of a well-known Butler–Volmer equation as follows²⁴

$$j = ai_0 \left(\frac{c}{c_{\text{ref}}} \right)^\gamma \left\{ e^{[\alpha_a F(\Phi_1 - \Phi_2 - U)/RT]} - e^{[-\alpha_c F(\Phi_1 - \Phi_2 - U)/RT]} \right\} \quad [15]$$

Because a continuously changes, as mentioned above, a relationship between a and the amount of conductive material (Pb or PbO₂) available in the electrode can be expressed as follows

$$a = a_{\text{max}} \left(\frac{Q}{Q_{\text{max}}} \right)^\xi \quad [16]$$

where Q is the local number of coulombs per unit volume of the electrode, Q_{max} is the maximum coulombs per unit volume that can be extracted from the electrode at a given electrolyte concentration, temperature, and discharge rate, and the power ξ is an empirical factor used to account for the way the product covers the electrode surface. During charge, an additional term is needed to account for the reverse reaction, which is expressed as

$$a \left(1 - \frac{Q}{Q_{\text{max}}} \right) = a_{\text{max}} \left(\frac{Q}{Q_{\text{max}}} \right)^\xi \left(1 - \frac{Q}{Q_{\text{max}}} \right) \quad [17]$$

The rate at which available active area changes depends on the rate at which the charge density Q changes with the reaction. Thus a balance on the charge density can be written as

$$\frac{\partial Q}{\partial t} = j \quad [18]$$

By the assumption of electroneutrality, the transfer current j is related to the current density in the liquid and solid phases as follows²⁴

$$j = - \frac{\partial i_1}{\partial x} = \frac{\partial i_2}{\partial x} \quad [19]$$

Also a relationship between the porosity ε and charge density Q can be established as follows

$$\frac{Q}{Q_{\text{max}}} = \frac{\varepsilon - \varepsilon_0}{\varepsilon_{\text{max}} - \varepsilon_0} \quad [20]$$

and

$$1 - \frac{Q}{Q_{\text{max}}} = \frac{\varepsilon_{\text{max}} - \varepsilon}{\varepsilon_{\text{max}} - \varepsilon_0} \quad [21]$$

Thus, only a set of five dependent variables is needed to be solved for each porous electrode, $-c$, ε , Φ_1 , Φ_2 , and i_2 , as given in Table I.

Table I shows the rearranged form of the governing equations for electrolyte concentration, electrolyte potential, solid phase potential, and porosity variation in all the four regions of a lead-acid cell. This is expressed by combining the derived equations for balance on electrolyte concentration, porosity and charge density, conservation of charge and volume, Ohm's law in solution and solid, electrode kinetics and transfer current relationship with solution, and solid phase current densities.

Simulation issues.—It could be realized that the mathematical model of the lead-acid cell involves simultaneous interaction of thermodynamic, kinetic, electrical, and mass transport phenomena. Due to this complex nature of the electrochemical behavior, the resulting model equations have to govern the interaction of multiphenomena, and the model typically requires a numerical simulation. Secondary battery models with similar mathematical simulation complexity are typically solved using a discretization method like the finite difference, finite element, or finite volume methods.

In this investigation, the model equations are solved using the three-point finite difference method with accuracy to the order of Δx^2 in the x direction. The numbers of internal node points used are 20 in each region of the lead-acid cell, as shown in Fig. 1, which add up to 80 internal node points that exclude node points at two boundaries and three interfaces. The resulting system of differential algebraic equations (DAEs) is solved using a DAE solver called Bulir-

sch Extrapolated Semi-Implicit Runge-Kutta (BESIRK) in Maple environment.²⁵ Because the model needs consistent initial conditions at time $t = 0$, a nonlinear algebraic equation solver called Newton is used in Maple environment for this purpose.²⁶⁻²⁸ 50 time steps are needed for the simulation of smooth performance curve during the charge, rest, or discharge process. Typically, it takes 1–3 min in Maple environment for the simulation of a discharge, rest, or charge curve using a personal computer with 2 Gbytes of random access memory and 2.3 GHz processor.

Modeling Corrosion Process

Modeling secondary batteries like lead-acid, lithium-ion, and nickel-metal-hydride systems has gained momentum to simulate process variables (voltage, power, energy, etc.) and intrinsic variables (solid phase concentration, electrolyte potential, local current density, etc.). The electrochemical engineering continuum model for the lead-acid battery was derived based on concentrated solution theory, porous electrode theory, modified Ohm's law, and other transport and kinetic phenomena.⁹⁻¹¹ Unlike Ni or Li systems, lead-acid battery has significant porosity variation as a function of time due to the sulfate formation at porous electrodes. It consists of four regions, as shown in Fig. 1, and has multiple partial differential equations in multiple domains to solve for process and intrinsic variables. Table I shows the governing equations for the first-principles-based lead-acid battery model that are used in this investigation.⁹ Table II shows the boundary and initial conditions used to solve for each governing equation given in Table I. For large discharge current and to obtain numerical convergence while using most of the available DAE solvers like Differential Algebraic System Solver²⁹ and BESIRK,²⁵ the initial conditions for Φ_1 and Φ_2 as a function of distance across the cell, x , should be evaluated using the model equations for the algebraic variables at time $t = 0$. Table III shows a list of kinetic and transport expressions used for solving the model. Table IV provides a detailed list of parameters involved in the model with the nomenclature and parameter values. The IC rate of charge or discharge corresponds to an absolute value of 15 mA/m². In this work, the lead-acid battery performance is studied at 100 mA/m² for about 400 s to explore the battery capability at high rates. The limiting factor that affects lead-acid battery life is the corrosion process that is noticed between the plate grid material and the positive active mass in the PbO₂ electrode. This corrosion process is also shown in Fig. 1. In this work, different approaches are followed to model this process.

Empirical approach.—First, the electronic conductivity of the PbO₂ electrode is empirically expressed as a function of N , the number of cycle. This function can be of the form

$$\sigma_{\text{PbO}_2} = \sigma_{\text{PbO}_2}^\alpha N^{\sigma_{\text{PbO}_2}^\beta} \quad [22]$$

where N is the number of cycle and $\sigma_{\text{PbO}_2}^\alpha$ and $\sigma_{\text{PbO}_2}^\beta$ are empirical constants. The electrochemical engineering model for the lead-acid battery has been solved with these kinetic expressions and compared with the same model without incorporating the corrosion mechanism.

I-R loss approach.—Next, an current–resistance (I - R) loss term to account for the increase in electronic resistance at the positive plate due to the formation and growth of passive corrosion layer is analyzed. Here, the modified Butler–Volmer electrochemical kinetic expression for the positive plate is expressed as follows

$$j_p = a_{\text{max}} i_{01, \text{ref}} \left(\frac{c}{c_{\text{ref}}} \right)^{\gamma_1} \left(\frac{\varepsilon - \varepsilon_{1,0}}{\varepsilon_{1, \text{max}} - \varepsilon_{1,0}} \right)^{\xi_1} \left\{ e^{[\alpha_1 F(\Phi_1 - \Phi_2 - U_p - j_p R_c / a_{\text{max}}) / RT]} - e^{[-\alpha_c F(\Phi_1 - \Phi_2 - U_p - j_p R_c / a_{\text{max}}) / RT]} \right\} \quad [23]$$

where R_c is the additional resistance to electron conduction due to the corrosion layer buildup.

Table II. Boundary and initial conditions for the governing equations.

Region	Boundary conditions	Initial conditions
Positive plate	$\left. \frac{\partial c}{\partial x} \right _{x=0} = 0 \text{ and } \varepsilon^{\text{ex1}} \left. \frac{\partial c}{\partial x} \right _{\Gamma_p^-} = \left. \frac{\partial c}{\partial x} \right _{\Gamma_p^+}$ $\left. \frac{\partial \Phi_2}{\partial x} \right _{x=0} = 0 \text{ and } \varepsilon^{\text{ex1}} \left. \frac{\partial \Phi_2}{\partial x} \right _{\Gamma_p^-} = \left. \frac{\partial \Phi_2}{\partial x} \right _{\Gamma_p^+}$ $\left. \frac{\partial \Phi_1}{\partial x} \right _{x=0} = -\frac{I_{\text{app}}}{\varepsilon^{\text{exm1}} \sigma_{\text{PbO}_2}} \text{ and } \left. \frac{\partial \Phi_1}{\partial x} \right _{l_p} = 0$ $\left. \frac{\partial \varepsilon}{\partial t} \right _{x=0} = \frac{a_1 j_p}{2F} \text{ and } \left. \frac{\partial \varepsilon}{\partial t} \right _{l_p} = \frac{a_1 j_p}{2F}$	$c _{t=0} = c_{\text{ref}}$
Reservoir	$\left. \frac{\partial c}{\partial x} \right _{l_p+\Gamma_r} = \varepsilon^{\text{ex3}} \left. \frac{\partial c}{\partial x} \right _{l_p+\Gamma_r^+}$ $\left. \frac{\partial \Phi_2}{\partial x} \right _{l_p+\Gamma_r} = \varepsilon^{\text{ex3}} \left. \frac{\partial \Phi_2}{\partial x} \right _{l_p+\Gamma_r^+}$	$\varepsilon _{t=0} = \varepsilon_{1,\text{max}}$ $c _{t=0} = c_{\text{ref}}$
Separator	$\varepsilon^{\text{ex3}} \left. \frac{\partial c}{\partial x} \right _{l_p+l_r+l_s} = \varepsilon^{\text{ex4}} \left. \frac{\partial c}{\partial x} \right _{l_p+l_r+l_s^+}$ $\varepsilon^{\text{ex3}} \left. \frac{\partial \Phi_2}{\partial x} \right _{l_p+l_r+l_s} = \varepsilon^{\text{ex4}} \left. \frac{\partial \Phi_2}{\partial x} \right _{l_p+l_r+l_s^+}$	$c _{t=0} = c_{\text{ref}}$
Negative plate	$\Phi_2 _{x=L} = \Phi_{2,\text{ref}}$ $\left. \frac{\partial \Phi_1}{\partial x} \right _{l_p+l_r+l_s} = 0 \text{ and } \left. \frac{\partial \Phi_1}{\partial x} \right _{x=L} = -\frac{I_{\text{app}}}{\varepsilon^{\text{exm4}} \sigma_{\text{Pb}}}$ $\left. \frac{\partial \varepsilon}{\partial t} \right _{l_p+l_r+l_s} = -\frac{a_2 j_n}{2F} \text{ and } \left. \frac{\partial \varepsilon}{\partial t} \right _{x=L} = -\frac{a_2 j_n}{2F}$	$c \left. \frac{\partial c}{\partial x} \right _{x=l_r} = 0$ $\varepsilon _{t=0} = \varepsilon_{4,\text{max}}$

Side reaction approach.— Finally, corrosion mechanism is incorporated as a side reaction in PbO₂ electrode kinetics. The side reaction that leads to the corrosion in the positive plate is expressed as



The lead in this reaction is from the grid material and not from the active mass. From this side reaction it is evident that the anodic corrosion decreases positive grid conductivity significantly over a

period of battery operations. To incorporate the effect of side reaction (Eq. 24) into the electrochemical kinetics of the main reactions given by Eq. 1 and 2, a modification to the Butler–Volmer electrochemical kinetic expression of the positive plate (given in Table III) is introduced as follows³⁰

$$j_p = j_1 + j_s \quad [25]$$

Table III. Transport and kinetic expressions used in the model.

Electrolyte
$D = 10^{-5} \times (1.75 + 260c)e^{(2174/298.15 - 2174/T)}$ $\kappa = ce^{(1.1104 + 199.475c - 16,097.781c^2 + 3916.95 - 99,406c - 721,860/T)}$
<p>Positive plate</p> $a_1 = \frac{\text{MW}_{\text{PbSO}_4}}{\rho_{\text{PbSO}_4}} - \frac{\text{MW}_{\text{PbO}_2}}{\rho_{\text{PbO}_2}}$ $j_p = a_{\text{max}} i_{01,\text{ref}} \left(\frac{c}{c_{\text{ref}}} \right)^{\gamma_1} \left(\frac{\varepsilon - \varepsilon_{1,0}}{\varepsilon_{1,\text{max}} - \varepsilon_{1,0}} \right)^{\xi_1} \{ e^{[\alpha_{a1} F(\Phi_1 - \Phi_2 - U_p)/RT]} - e^{[-\alpha_{c1} F(\Phi_1 - \Phi_2 - U_p)/RT]} \}$ $U_p = 1.9228 + 0.147519 \log(m) + 0.063552 \log(m)^2 + 0.073772 \log(m)^3 + 0.033612 \log(m)^4$ $m = 1003.22c + 0.355 \times 10^5 c^2 + 0.217 \times 10^7 c^3 + 0.206 \times 10^9 c^4$
<p>Negative plate</p> $a_2 = \frac{\text{MW}_{\text{PbSO}_4}}{\rho_{\text{PbSO}_4}} - \frac{\text{MW}_{\text{Pb}}}{\rho_{\text{Pb}}}$ $j_n = a_{\text{max}} i_{04,\text{ref}} \left(\frac{c}{c_{\text{ref}}} \right)^{\gamma_4} \left(\frac{\varepsilon - \varepsilon_{4,0}}{\varepsilon_{4,\text{max}} - \varepsilon_{4,0}} \right)^{\xi_4} \{ e^{[\alpha_{a4} F(\Phi_1 - \Phi_2 - U_n)/RT]} - e^{[-\alpha_{c4} F(\Phi_1 - \Phi_2 - U_n)/RT]} \}$ $U_n = 0$

Table IV. Parameters used for the simulation.

Electrolyte	
Acid concentration, c_{ref}	$4.9 \times 10^{-3} \text{ mol cm}^{-3}$
Transference number, t_+	0.90
Temperature, T	298.15 K
Partial molar volume of electrolyte, V_e	$45 \text{ cm}^3 \text{ mol}^{-1}$
Partial molar volume of solvent, V_o	$17.5 \text{ cm}^3 \text{ mol}^{-1}$
Molecular weight of PbSO_4 , $\text{MW}_{\text{PbSO}_4}$	$303.25 \text{ g mol}^{-1}$
Density of PbSO_4 , ρ_{PbSO_4}	6.3 g cm^{-3}
Potential of the reference electrode (which can be the same kind as working electrode), $\Phi_{2,\text{ref}}$	0
Mean molar activity coefficient, f	0.90
Positive plate	
Half-thickness of plate, l_p	0.06 cm
Maximum charge state, Q_{max}	3500 C cm^{-3}
Maximum specific active surface area of electrode, a_{max}	$100 \text{ cm}^2 \text{ cm}^{-3}$
Exchange current density at c_{ref} , $i_{01,\text{ref}}$	$1 \times 10^{-3} \text{ A cm}^{-2}$
Lead dioxide conductivity, σ_{PbO_2}	4800 S cm^{-1}
Anodic transfer coefficient for positive plate, α_{a1}	1.0
Cathodic transfer coefficient for positive plate, α_{c1}	1.0
Concentration exponent for positive plate, γ_1	2.0
Morphology parameter for positive plate, ξ_1	2.0
Porosity at full charge, $\varepsilon_{1,\text{max}}$	0.5
Porosity at zero charge, $\varepsilon_{1,0}$	0.2
Exponent on porosity, ex1	1.5
Empirically determined constant for tortuosity of the solid matrix, exm1	0.5
Reservoir	
Thickness of reservoir, l_r	0.05 cm
Separator	
Thickness of separator, l_s	0.03 cm
Porosity, ε_{sep}	0.55
Exponent on porosity, ex3	1.5
Negative plate	
Half-thickness of plate, l_{neg}	0.06 cm
Maximum charge state, Q_{max}	3700 C cm^{-3}
Maximum specific active surface area of electrode, a_{max}	$100 \text{ cm}^2 \text{ cm}^{-3}$
Exchange current density at c_{ref} , $i_{04,\text{ref}}$	$1 \times 10^{-3} \text{ A cm}^{-2}$
Lead dioxide conductivity, σ_{Pb}	$48,000 \text{ S cm}^{-1}$
Anodic transfer coefficient for negative plate, α_{a4}	1.5
Cathodic transfer coefficient for negative plate, α_{c4}	0.5
Concentration exponent for negative plate, γ_4	2.0
Morphology parameter for negative plate, ξ_4	1.0
Porosity at full charge, $\varepsilon_{4,\text{max}}$	0.5
Porosity at zero charge, $\varepsilon_{4,0}$	0.2
Exponent on porosity, ex4	1.5
Empirically determined constant for tortuosity of the solid matrix, exm4	0.5
Limiting current density for negative plate, j_{lim}	-100 A cm^{-3}

$$j_1 = a_{\text{max}} i_{01,\text{ref}} \left(\frac{c}{c_{\text{ref}}} \right)^{\gamma_1} \left(\frac{\varepsilon - \varepsilon_{1,0}}{\varepsilon_{1,\text{max}} - \varepsilon_{1,0}} \right)^{\xi_1} \left\{ e^{[\alpha_{a1} F(\Phi_1 - \Phi_2 - U_p)/RT]} - e^{[-\alpha_{c1} F(\Phi_1 - \Phi_2 - U_p)/RT]} \right\} \quad [26]$$

$$j_s = a_{\text{max}} i_{01,\text{side}} e^{[\alpha_{a1} F(\Phi_1 - \Phi_2 - U_{\text{ref,side}})/RT]} \quad [27]$$

where $U_{\text{ref,side}}$ and $i_{01,\text{side}}$ are the reference potential and exchange current density for the side reaction.

Results and Discussion

The complete model equations in Table I are solved using the finite difference method in Maple environment. In addition to the process variable the intrinsic variables are also plotted for discussion. Figure 2 shows the electrolyte concentration distribution across the electrode as a function of discharge time. The concentration of

the electrolyte at the positive electrode drops toward zero during discharge and thus controls the end of the discharge process. A similar observation can also be obtained from the plot of overpotential ($\Phi_1 - \Phi_2$) as a function of discharge time at various boundaries and interfaces of the lead-acid cell, as shown in Fig. 3. It can be seen that the overpotential drop in the positive electrode is nearly 200–250 mV, whereas in the negative electrode the drop is only between 50 and 100 mV. The porosity variations at the positive and negative electrodes are shown in Fig. 4a and b. Though the initial porosity for both the electrodes is 0.5, it drops by 40% for the positive electrode due to the formation of lead sulfate and water molecules where it is only a drop between 30 and 35% for the negative electrode due to the lead sulfate formation.⁹ The lead sulfate formation decreases the pore volume which in turn decreases the electrolyte transport into the positive electrode and increases the resistances for mass trans-

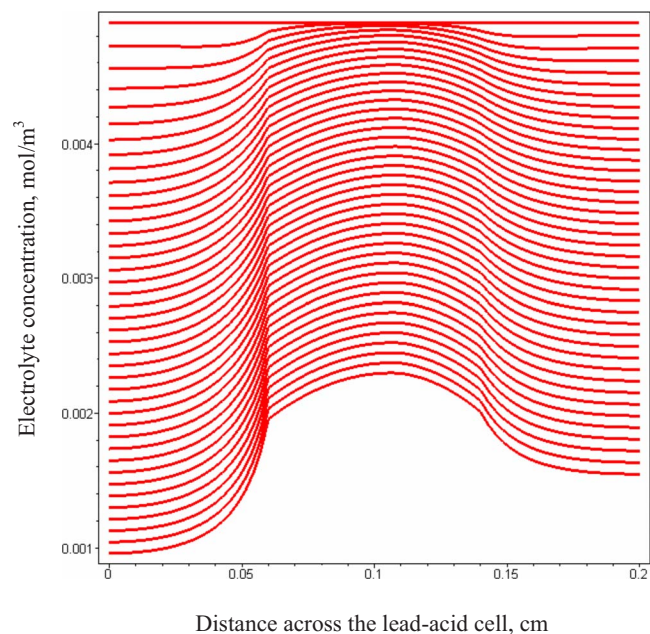


Figure 2. (Color online) Profiles of electrolyte concentration distribution across the lead-acid cell as a function of discharge time.

port and electrochemical kinetics. This phenomenon results in positive plate failure compared to the electrochemical performances of the negative plate. The computation time taken for the simulation of a single discharge curve of the lead-acid battery model is 1–2 min. Similarly, for the rest period and the charge curve simulations, they are 1.5 and 1 min, respectively, in Maple environment.

Figure 5 shows a comparison between the charge and discharge profiles from the model shown in Table I and the model that accounts for corrosion, as discussed in the Modeling Corrosion Process section. A considerable loss in charge or discharge potential can be noticed in Fig. 5. This is due to the effect of the initial corrosion layer that is formed between the active material and the grid material of the positive plate. Among the three approaches the approach

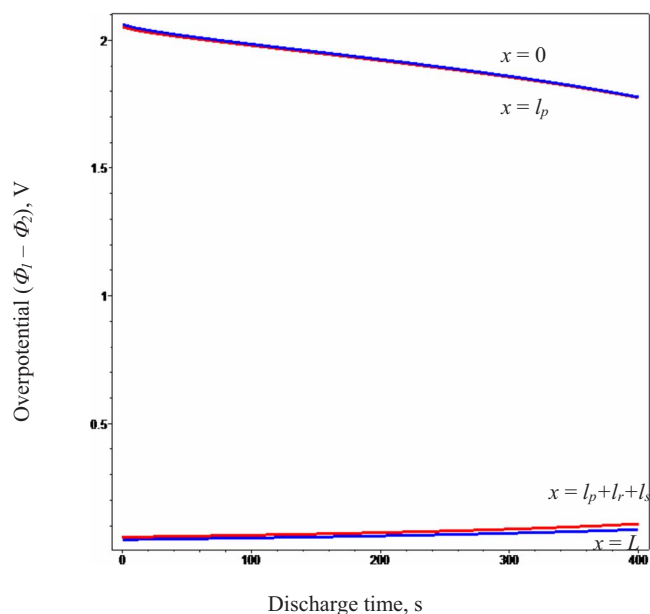


Figure 3. (Color online) Profiles of overpotential distribution as a function of discharge time at various boundaries and interfaces of the lead-acid cell.

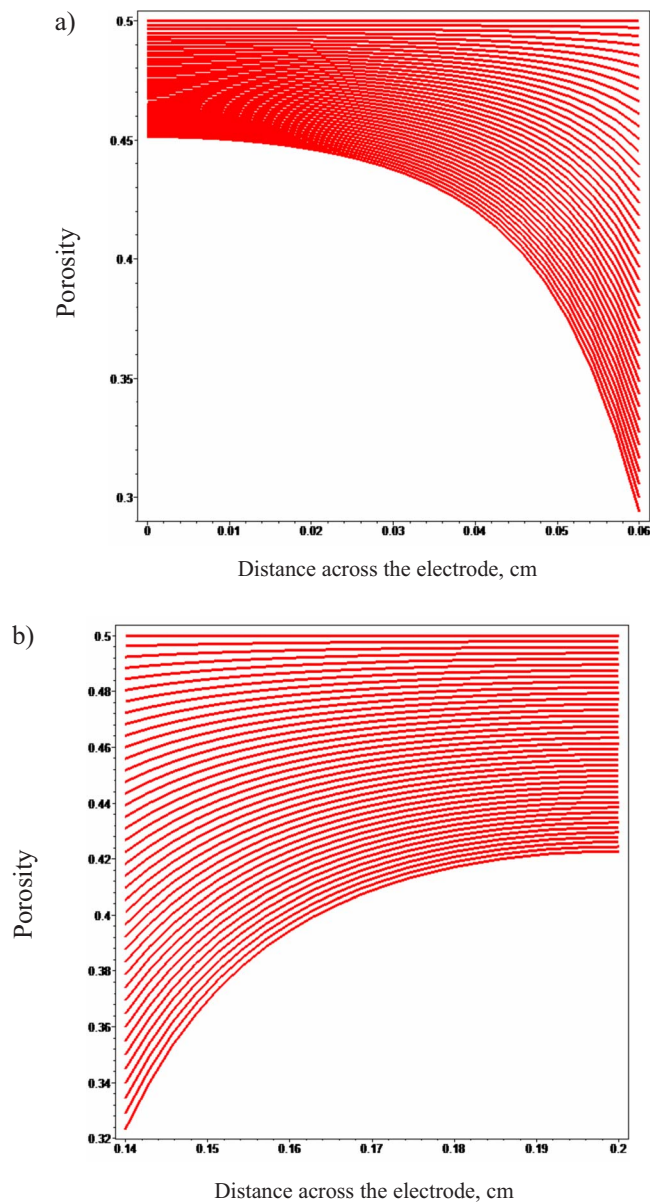


Figure 4. (Color online) Profiles of electrode porosity distribution across the porous electrodes of the lead-acid cell as a function of discharge time: (a) Positive plate and (b) negative plate.

that takes account of corrosion phenomena as a side reaction predicts more losses in both charge and discharge curves. The I - R loss approach predicts a uniform loss in charge and discharge performances as a function of time. Because the plot made is for the initial cycle, the other approach which uses an empirical equation as a function of electronic conductivity at the positive plate did not predict considerable losses. It can be concluded that expressing corrosion as a side reaction seems to be more realistic than the other two approaches.

The computation time taken for the simulation of single cycle performance of the lead-acid battery model using the first approach, where a modified Butler–Volmer equation has been accounted for the side reaction, is 1–2 min. Similarly for the other approaches with PbO_2 conductivity variation as a function of N and I - R loss term, it is 2 and 3 min, respectively. Because the approach with I - R loss term needs an additional equation to be solved in each porous electrode, it requires more computational time compared to the other two approaches.

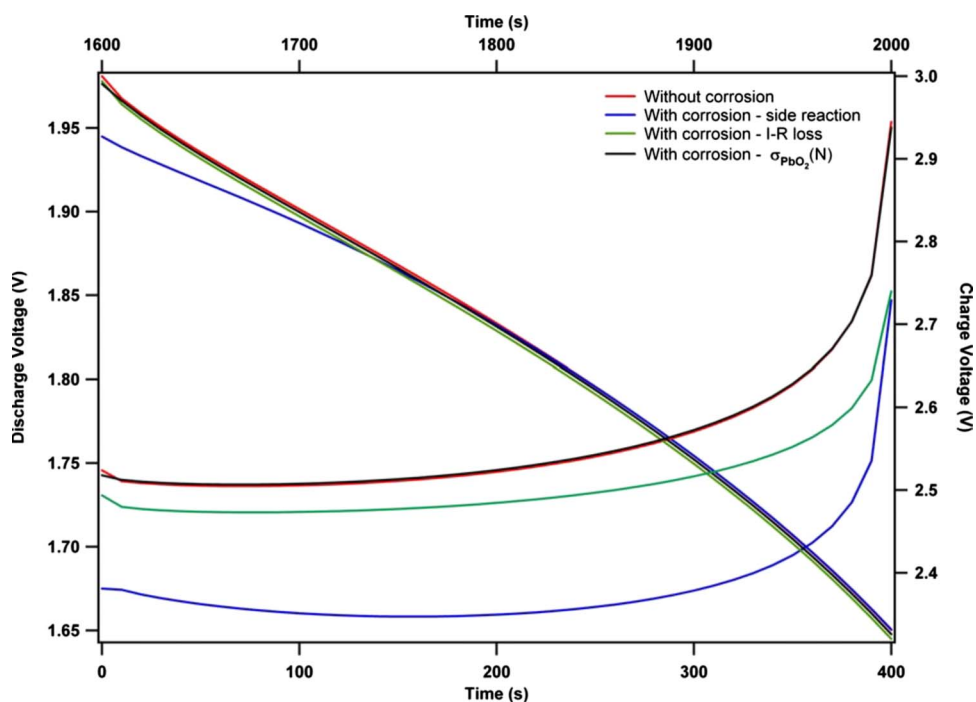


Figure 5. (Color online) Comparison of discharge, rest, and charge performances between models with and without corrosion mechanism.

The model prediction for corrosion agrees qualitatively with the experimental data.^{2-4,31} The latest experimental effort³¹ does not report charge-discharge curves to directly compare with the results obtained from this investigation. However, the researchers have reported a decrease in electronic conductivity and less efficient conduction. This is consistent with the results reported in this investigation (as shown in Fig. 5). Also, the corrosion layer thickness is related to the number of cycles. Currently, work is in progress to run these models for number of cycles N , and future publications report comparisons with experimental data.

Conclusion

A mathematical model for the lead-acid battery with due consideration for the effect of corrosion that occurs at the interface between active mass and grid material of the positive plate is developed. This corrosion process has been modeled using three different approaches, namely, (i) electronic conductivity of the positive plate expressed as an empirical function in N , (ii) I - R loss term to account for the increase in electronic resistance due to the formation and growth of the passive corrosion layer, and (iii) corrosion as a side reaction at the positive plate. The third approach that accounts for corrosion as a side reaction in the positive plate is intuitively considered as a better model over the other approaches. With this modeling capability, it is also identified that the model with corrosion as a side reaction might be used to study the effect of corrosion on battery cycle performance.

Acknowledgments

Sincere acknowledgments are due to the Oronzio de Nora Industrial Electrochemistry Postdoctoral Fellowship of the Electrochemical Society without which this work could have not been possible.

Tennessee Technological University assisted in meeting the publication costs of this article.

List of Symbols

α_{a1}	anodic transfer coefficient for the positive plate
α_{a4}	anodic transfer coefficient for the negative plate
α_{c1}	cathodic transfer coefficient for the positive plate
α_{c4}	cathodic transfer coefficient for the negative plate
a_{\max}	maximum specific active surface area of the electrode, $\text{cm}^2 \text{cm}^{-3}$

c_{ref}	concentration of the electrolyte, mol cm^{-3}
exm1	empirically determined constant for tortuosity of the solid matrix for the positive plate
exm4	empirically determined constant for tortuosity of the solid matrix for the negative plate
ex1	exponent on porosity for the positive plate
ex3	exponent on porosity for the separator
ex4	exponent on porosity for the negative plate
f	mean molar activity coefficient
γ_1	concentration exponent for the positive plate
γ_4	concentration exponent for the negative plate
ε_{sep}	porosity of the separator
$\varepsilon_{1,\max}$	porosity for the positive plate at full charge
$\varepsilon_{1,0}$	porosity for the positive plate at zero charge
$\varepsilon_{4,\max}$	porosity for the negative plate at full charge
$\varepsilon_{4,0}$	porosity for the negative plate at zero charge
$i_{01,\text{ref}}$	exchange current density of the positive plate at c_{ref} , A cm^{-2}
$i_{04,\text{ref}}$	exchange current density of the negative plate at c_{ref} , A cm^{-2}
j_{lim}	limiting current density for the negative plate, A cm^{-3}
l_{neg}	half-thickness of the negative plate, cm
l_{p}	half-thickness of the positive plate, cm
l_{r}	thickness of the reservoir, cm
l_{s}	thickness of the separator, cm
MW_{PbSO_4}	molecular weight of PbSO_4 , g mol^{-1}
ξ_1	morphology parameter for the positive plate
ξ_4	morphology parameter for the negative plate
ρ_{PbSO_4}	density of PbSO_4 , g cm^{-3}
σ_{Pb}	lead dioxide conductivity, S cm^{-1}
σ_{PbO_2}	lead dioxide conductivity, S cm^{-1}
$\Phi_{2,\text{ref}}$	potential of the reference electrode, V
Q_{\max}	maximum charge state of the porous electrode, C cm^{-3}
t_{\pm}	transference number of the electrolyte
T	temperature of the electrolyte, K
V_{e}	partial molar volume of the electrolyte, $\text{cm}^3 \text{mol}^{-1}$
V_{o}	partial molar volume of the solvent, $\text{cm}^3 \text{mol}^{-1}$

References

1. C. M. Shepherd, *J. Electrochem. Soc.*, **112**, 657 (1965).
2. D. Simonsson, *J. Appl. Electrochem.*, **3**, 261 (1973).
3. D. Pavlov, *J. Electroanal. Chem.*, **72**, 319 (1976).
4. K. Micka and I. Rousar, *Electrochim. Acta*, **21**, 599 (1976).
5. P. Horvath, P. Jedlovsky, and M. Benedek, *J. Power Sources*, **8**, 41 (1982).
6. A. D. Turner and P. T. Moseley, *J. Power Sources*, **9**, 19 (1983).
7. G. Sunu, in *Electrochemical Cell Design*, R. E. White, Editor, pp. 357-376, Plenum, New York (1984).
8. S. Atlung and B. Fastrup, *J. Power Sources*, **13**, 39 (1984).
9. H. Gu, T. V. Nguyen, and R. E. White, *J. Electrochem. Soc.*, **134**, 2953 (1987).
10. P. Ekdunge, K. V. Rybalka, and D. Simonsson, *Electrochim. Acta*, **32**, 659 (1987).

11. P. Ekdunge and D. Simonsson, *J. Appl. Electrochem.*, **19**, 127 (1989); , **19**, 136 (1989).
12. T. V. Nguyen, R. E. White, and H. Gu, *J. Electrochem. Soc.*, **137**, 2998 (1990).
13. R. M. LaFollette and D. N. Bennion, *J. Electrochem. Soc.*, **137**, 3701 (1990).
14. P. Ekdunge, *J. Power Sources*, **46**, 251 (1993).
15. D. Baert and A. Vervaet, *Electrochim. Acta*, **44**, 3491 (1999).
16. H. A. Catherino, J. F. Burgel, A. Rusek, and F. Feres, *J. Power Sources*, **80**, 17 (1999).
17. M. G. Semenenko, *Russ. J. Electrochem.*, **40**, 98 (2004).
18. H. Doring, J. Garche, H. Dietz, and K. Wiesener, *J. Power Sources*, **30**, 41 (1990).
19. D. Pavlov, *J. Power Sources*, **53**, 9 (1995).
20. R. J. Ball, R. Evans, and R. Stevens, *J. Power Sources*, **103**, 207 (2002).
21. R. J. Ball, R. Evans, and R. Stevens, *J. Power Sources*, **103**, 213 (2002).
22. W. R. Osório, C. S. C. Aoki, and A. Garcia, *J. Power Sources*, **185**, 1471 (2008).
23. B. Culpin and D. A. J. Rand, *J. Power Sources*, **36**, 415 (1991).
24. J. S. Newman, *Electrochemical Systems*, 3rd ed., Wiley Interscience, Hoboken, NJ (2004).
25. <http://people.clarkson.edu/~chengweb/faculty/taylor/>, (last accessed August 2009)..
26. D. Schwalbe, H. A. Kooijman, and R. Taylor, *Maple Tech*, **3**, 47 (1996).
27. V. Boovaragavan and V. R. Subramanian, *Electrochem. Commun.*, **9**, 1772 (2007).
28. B. Wu and R. E. White, *Comput. Chem. Eng.*, **25**, 301 (2001).
29. K. E. Brenan, S. L. Campbell, and L. R. Petzold, *Numerical Solution of Initial-Value Problems in Differential-Algebraic Equations*, North-Holland, New York (1989).
30. P. Ramadass, P. M. Gomadam, R. E. White, and B. N. Popov, *J. Electrochem. Soc.*, **151**, A196 (2004).
31. R. J. Ball, R. Kurian, R. Evans, and R. Stevens, *J. Power Sources*, **111**, 23 (2002).